Jordanian Journal of Computers and Information Technology (JJCIT), Vol. 11, No. 02, June 2025.

GROUND-TO-SATELLITE FSO COMMUNICATION: EVALUATING MODULATION TECHNIQUES UNDER CLOUD AND TURBULENCE EFFECTS

Mouna Garai[1], Maha Sliti[1] and Abdelrahman Elfikky[2]

(Received: 28-Dec.-2024, Revised: 26-Mar.-2025 and 3-Apr.-2025, Accepted: 5-Apr.-2025)

ABSTRACT

Free-space optical (FSO) communication is a vital solution to meet the growing demand for high-bandwidth satellite-to-ground communication, offering advantages, such as higher data rates and security compared to traditional RF systems. However, its performance is significantly affected by meteorological conditions, particularly cloud formations (e.g. cirrus, cumulus and stratocumulus) and atmospheric turbulence, which cause signal attenuation, scattering and phase distortions. Addressing these challenges through better understanding and mitigation strategies is essential to ensure reliable and efficient performance of FSO systems under various atmospheric conditions. In this study, we evaluated the performance of ground- to-satellite FSO systems under varying atmospheric turbulence and cloud conditions using the OptiSystem simulator. We analyze multiple modulation techniques, including Quadrature Phase Shift Keying (QPSK), 8-Phase Shift Keying (8PSK), 16PSK and 16-Quadrature Amplitude Modulation (16QAM), to assess their resilience based on link range, bit-error rate (BER), quality factor, optical signal-to-noise ratio (OSNR) and error-vector magnitude (EVM). The results demonstrate that QPSK outperforms higher- order modulation schemes in high-attenuation environments, maintaining the lowest BER and highest quality factor, making it the most suitable choice for FSO communication in satellite networks. These findings provide critical insights into the optimization of modulation strategies for robust and reliable ground-to-satellite optical links.

KEYWORDS

Atmospheric turbulence, Cloud attenuation, FSO, Gamma-Gamma turbulence model, Modulation techniques, Optical ground-to-satellite link.

1. INTRODUCTION

Free-space Optical (FSO) communication has emerged as a cornerstone technology in modern telecommunications, widely recognized for its ability to transmit data at exceptional speeds with minimal latency [1]-[4]. This capability makes FSO an indispensable component in telecommunication networks, where it is crucial to enable high-speed Internet connectivity and support data-intensive applications. Beyond its conventional uses, FSO demonstrates remarkable adaptability in various domains, including real-time surveillance, high-definition video broadcasting and bridging the digital divide in underserved and rural regions [5]-[6]. These diverse applications underscore the technology's potential to address complex communication challenges while offering scalable and efficient solutions.

FSO-communication links are highly sensitive to environmental factors, such as fog, rain and snow, which can significantly attenuate the optical signal [7]-[19]. Furthermore, atmospheric turbulence causes beam scintillation and wavefront distortions, leading to deterioration in link quality [20]-[22]. Thus, the adoption of FSO technology in satellite-to-ground communications is hindered by significant challenges posed by atmospheric conditions, including cloud cover and turbulence [23]-[24].These meteorological factors alter the reliability of the communication link, leading to attenuation and signal degradation. This occurs primarily because of photon absorption and scattering caused by the presence of dense cloud formations and water droplets. Moreover, atmospheric turbulence, induced by random fluctuations in temperature and pressure along the signal's propagation path, further compounds these issues. Turbulence introduces random phase distortions, scintillations and beam wanders, severely impacting the system's overall performance and dependability. Overcoming these atmospheric hurdles is vital to achieve the full potential of FSO systems in challenging operational environments.

1. M. Garai and M. Sliti are with University of Carthage, Higher School of Communication of Tunis (SUP'COM), LR11TIC04, Communication Networks and Security Research Lab. & LR11TIC02, Green and Smart Communication Systems Research Lab, Tunisia. Emails: mouna.garai@gmail.com and {slitimaha@gmail.com; maha.sliti@istic.ucar.tn}.
2. A. Elfikky is with Arab Academy for Sci. and Technol. and Maritime Support, Alexandria, Egypt. Email: afikky@ucsc.edu

This study examines the influence of turbulence and various types of cloud, such as stratocumulus, cumulus and cirrus clouds, on ground-to-satellite FSO systems. We also use OptiSystem to simulate various modulation schemes, such as Quadrature Phase Shift Keying (QPSK), 8-Phase Shift Keying (8PSK), 16-PSK and 16-Quadrature Amplitude Modulation (16-QAM), which provide important insights into the system's performance under different cloud types in the presence of turbulence. We then compare their robustness using the bit-error rate (BER), quality factor, optical signal-to-noise ratio (OSNR) and error-vector magnitude (EVM). The findings show that QPSK modulation is the optimal choice for FSO communication in satellite networks with cloud-induced attenuation levels. The study revealed that QPSK regularly exceeds alternative modulation techniques, delivering the lowest Bit Error Rate (BER) even in challenging scenarios. QPSK is particularly effective in evaluating the influence of transmitted power, attaining significantly low bit-error rate (BER) values even at low power levels. QPSK and 16-PSK offer improved performance and higher quality-factor values, particularly at shorter distances. QPSK consistently has lower EVM values, demonstrating greater noise tolerance even at low OSNR levels. QPSK is recommended as the modulation technology for FSO communication over satellite links, due to its ability to maintain reliable communication even in unfavorable conditions.

We can summarize the current study's contributions as follows:

- We develop a comprehensive FSO-channel model that integrates the effects of both atmospheric turbulence and cloud attenuation. Unlike conventional models, our approach distinguishes between different cloud types (e.g. cirrus, cumulus, stratocumulus), enabling a more precise characterization of signal degradation.
- Our study systematically compares multiple modulation schemes (QPSK, 8-PSK, 16-PSK and 16-QAM) under identical and realistic atmospheric conditions. This analysis highlights the trade-offs between spectral efficiency and robustness, thereby providing clear insights into optimal modulation strategies for ground-to-satellite links.
- The simulation results obtained through the OptiSystem platform are rigorously validated against analytical models derived from established channel theories. This dual validation confirms the accuracy and reliability of key performance metrics, such as Bit-Error Rate, Optical Signal-to-Noise Ratio and Error-Vector Magnitude.

The following sections are organized as follows: Section 2 examines existing mitigation approaches to reduce the impact of cloud formation on the performance of FSO systems. Section 3 explores the impact of attenuation caused by various types of clouds, as well as an examination of the known models and methodologies used to measure these effects. Section 4 provides a comprehensive description of the design of the proposed ground-to-satellite FSO system, taking into account different cloud conditions and presents the different modulation approaches considered for the proposed ground-satellite FSO system. Section 5 presents the obtained simulation results and provides the analytical validation of the simulation results. Section 6 shows a list of abbreviations used in the study. Finally, Section 7 concludes the paper.

2. RELATED WORK

Cloud-induced attenuation in satellite-based free-space optical communications is an important research area [25]-[31]. Numerous studies have provided valuable information on modeling, understanding and mitigation of the impact of clouds on FSO links.

Using the meteorological ERA-Interim database, the authors in [32] examined the availability of links in various regions of Japan. They suggested a site-diversity strategy to enhance system availability and offer practical advice for resolving cloud-induced issues in FSO communications. The authors of [33] investigated cloud-induced attenuation in satellite-based free-space optical communications, with a particular emphasis on regions of Japan. The FSO channel model is selected based on the log-normal distribution, which enhances the understanding of the probabilistic nature of cloud-induced attenuation. The authors of [34] simulated a 30 Gbps ground-to-geostationary satellite-FSO communication link that accommodates a variety of cloud states and atmospheric impacts. The results illustrate the efficacy of a 2x2 MIMO system that employs coherent detection and QPSK modulation, with a particular emphasis on the minimal occurrence of symbol errors in a variety of cloud and weather conditions. An analytical model for estimating the probability of cloud-free line-of-sight

(CFLOS) in optical satellite links is introduced in [35]. This model is predicated on the assumption of a lognormal distribution for Integrated Liquid Water Content (ILWC). This approach offers a practical approach to effectively anticipating and resolving cloud-related challenges. The authors of [36] suggested the development of hybrid free-space optical/radio frequency (FSO/RF) systems to relay satellite communication from high-altitude platforms. This approach uses rate adaptation to adjust the data rates in response to channel-condition oscillations. Additionally, an examination of perfect inter-symbol interference (ISI) caused by cloud effects is conducted, which offers valuable insights into the constraints and restrictions that clouds place on FSO communication lines. The authors of [37] investigated the impact of cloud attenuation on the performance of optical wireless networks. They evaluated various cloud varieties. The research underscores the significance of wavelength-dependent attenuation and illustrates that stratocumulus clouds have the most significant influence on signal transmission. The meteorological ERA-Interim database is employed by the authors in [38] to determine the monthly average cloud attenuation over Japan. Based on the simulation results, the selection of a diverse array of sites from the proposed pool of options leads to a high level of system availability, which assists optical satellite-communication systems in mitigating the effects of cloud-induced attenuation. A comprehensive performance analysis of the atmospheric influence on visibility in FSO systems is conducted in [39], with a particular emphasis on ground station-satellite communications. The objective of the investigation is to establish correlations between visibility and climatic events, including factors, such as precipitation and snowfall. A study conducted in [40] examined the probability of the failure of integrated ground-air-space free-space optical communication lines when various models of atmospheric turbulence are employed. The article provides closed-form equations for cumulative distribution functions (CDFs) and probability density functions (PDFs). These equations take into account the zenith angle, atmospheric disturbances, the channel condition and the configuration of the links. The study offers a comprehensive analysis of the effectiveness of integrated FSO links, accounting for atmospheric attenuation, turbulence, angle of arrival fluctuations and targeting error. The evaluation of cloud-induced optical attenuation is the subject of [41]. This article suggested a comprehensive model that takes into account the influence of clouds on transmitted optical beams. Cloud-induced dispersed optical power is evaluated in this study through the application of modified gamma-particle size distributions (PSDs) and Mie theory. Cirrus clouds and their likelihood of formation, as well as their impact on FSO transceivers situated at elevated altitudes, are the primary focus. This research makes a substantial contribution to our comprehension of the impact of various atmospheric conditions on FSO communication systems, which encompasses both deep-space and near-Earth scenarios. Two distinct models for the scheduling of space-to-ground optical communication that incorporate uncertainty are presented in [42]. The first model employs robust optimization with a moment-based ambiguity set, while the second model employs robust optimization with a polyhedral uncertainty set. The study illustrates the efficacy of formulations that consider uncertainty when employing computational analysis on a real-world communication system, particularly in the context of cloud-cover predictions. The models that have been presented offer critical insights for the scheduling of space-to-ground optical communication systems by acknowledging the dynamic and variable character of the cloud cover.

Several studies have investigated the performance of various modulation schemes in FSO communication systems under atmospheric turbulence. For example, [43] compared several formats, including OOK, BPSK, DPSK, QPSK and 8-PSK and found that BPSK generally provides the lowest BER under severe turbulence. [44] evaluated the performance of schemes, such as BPSK-SIM, DPSK, DPSK-SIM, Polarization Shift Keying and M-ary Pulse Position Modulation and concluded that DPSK often achieves the best outage probability and higher channel capacity under turbulent conditions. In another study, [45] compared PPM, OOK, Differential Pulse Interval Modulation and Dual Header Pulse Interval Modulation in various weather scenarios and observed that PPM and OOK-NRZ generally deliver better BER performance. Recent research in FSO satellite networks has addressed key system-level issues. For example, [46] conducted a link-budget analysis for FSO satellite networks, providing valuable insights into power allocation under various atmospheric conditions. Furthermore, Liang et al. [47] performed a performance analysis of FSO satellite networks that examined transmission power and latency, while Liang et al. [48] explored the trade-off between latency and transmission power in networks with multiple intercontinental connections. These studies provide a strong foundation for the design and optimization of FSO satellite networks.

Although much of the existing literature focused on terrestrial FSO links, our work specifically

addresses the challenges of long-range ground-to-satellite communication, including high free-space path loss and atmospheric variability across different altitudes. Using advanced simulation tools, such as OptiSystem, we evaluated detailed performance metrics, such as BER, Q factor and EVM for various modulation schemes. This component-level analysis complements the network-level evaluations found in the literature, providing additional insights necessary for optimizing FSO system performance in practical deployment scenarios.

Table 1. Comparative overview of research in satellite-based free-space optical (FSO) communications under atmospheric conditions.

Ref.	Methodology	Modeling Technique	Parameters Considered	Data Source
[32]	Investigation of site-diversity scheme for enhanced system availability.	Not specified	Clouds, atmospheric turbulence	Meteorological ERA-Interim database [49]
[33]	Presentation of a novel distribution model of monthly cloud attenuation for several regions in Japan.	Log-normal distribution	Monthly cloud attenuation, CLWC	ERA-Interimal Meteorologic database
[34]	Simulation of a 30 Gbps satellite-FSO communication link. Consideration of atmospheric effects, like different cloud types. Use of a 2×2 MIMO system with QPSK modulation and coherent detection.	Not specified	Haze, fog, cloud types (stratus, cumulus, cumulonimbus), atmospheric turbulence, intensity scintillation	Not specified
[35]	Prediction of visibility/range of FSO link due to different cloud conditions.	Not specified	Link length, transmitted power, data rate, cloud types	Not specified
[36]	Presentation of analytical models for Cloud-Free Line-of-Sight (CF- LOS) probability. Evaluation of joint CFLOS statistics.	Not specified	Elevation angle, ground-station altitude, spatial variability of clouds	Not specified
[56]	Addressing the design of hybrid FSO/RF systems for high-altitude platform (HAP)-aided relaying satellite communication.	Rate-adaptation design	Beam-spreading loss, cloud attenuation, atmospheric turbulence, pointing misalignment	Not specified
[37]	Investigation of bit-error rate performance of intensity-modulated FSO with direct detection (IM/DD) in single-input single- output (SISO) due to beam broadening at the receiver caused by cloud.	IM/DD with direct detection & Perfect ISI due to beam broadening by clouds	Not specified	Not specified
[38]	Study of the influence of cloud attenuation on the performance of optical wireless links.	Not specified	Received power, visibility range, cloud type	Not specified
[39]	Study of a placement method of optical ground stations (OGSs) to realize site diversity in optical satellite-to-ground communications under cloud attenuation.	Greedy heuristic method	Monthly average cloud attenuation	Meteorological ERA-Interim database
[40]	Performance analysis for atmospheric influence on visibility in Free Space Optical Communications (FSOC).	Not specified	Atmospheric events (rain, snow), relationships to visibility	Not specified
[41]	Analysis of the outage probability of integrated ground-air-space FSO communication links for different atmospheric turbulence channel models.	Lognormal, Gamma exponentiated Weibull distributed channel models	Zenith angle, channel state, deviations, altitude, beam waist, …etc.	Not specified
[42]	Estimation of cloud-induced optical attenuation over near-Earth and deep-space FSO-communication systems.	Optical thickness parameter, modified gamma PSD, Mie theory	Type of atmospheric clouds, ground-space FSO link distances	Not specified
[50]	Provision of two alternative models of uncertainty for cloud-cover predictions. A robust optimization model with a polyhedral uncertainty set and a distributionally robust optimization model with a moment-based ambiguity set.	Robust optimization, distributionally robust optimization	Cloud-cover predictions, satellite operation scheduling	Official weather forecasts

Furthermore, while existing studies primarily emphasized BPSK and DPSK for their robustness, our work focuses on QPSK modulation for ground-to-satellite FSO links. Although QPSK may be slightly more sensitive to atmospheric disturbances than BPSK, it offers a substantial advantage in terms of spectral efficiency, an important factor for high-data-rate applications. The literature indicates that, while BPSK achieves the lowest BER under severe turbulence, its lower spectral efficiency limits its utility in bandwidth-constrained environments. DPSK, on the other hand, offers a balanced trade-off, but often requires more complex receiver designs. Our results demonstrate that QPSK delivers an acceptable BER while significantly increasing data throughput, making it a compelling option for space-to-ground communications. In addition, our detailed comparative evaluation of multiple

modulation techniques under realistic channel conditions, combined with rigorous simulation and analytical validation, clearly demonstrates the superior performance of QPSK. This distinct integration of simulation and analytical validation not only reinforces the reliability of our findings, but also sets our research apart from the existing literature.

Table 1 compares the different approaches considered in the literature to mitigate the impact of clouds on FSO links.

3. FSO CHANNEL MODEL

FSO communication systems are extremely sensitive to atmospheric conditions, which can dramatically reduce signal quality and system performance. This section gives a complete FSO-channel model that includes both atmospheric-turbulence and cloud-attenuation effects.

3.1 Atmospheric Turbulence

Atmospheric turbulence is a random phenomenon produced by differences in temperature and pressure along the transmission channel. Turbulence causes fluctuations in the temperature, pressure and, most importantly, the refractive index of the air. These changes in the refractive index affect the transmission of optical signals, resulting in scintillation, which is the fluctuation of the intensity of transmitted light.

In free-space optical satellite ground communication, the gamma-gamma distribution is commonly used to characterize the fluctuating received optical power (I) due to atmospheric turbulence. This model is recommended over others, because it successfully combines both small- and large-scale turbulence effects, making it applicable to a wide variety of turbulence situations, from moderate to high. The gamma-gamma model is particularly useful in satellite-ground communication because of the various turbulence levels experienced as the optical signal passes through several atmospheric layers, each with specific turbulence characteristics.

The gamma-gamma distribution's probability density function (PDF) is as follows ([52]):

$$p_I(I) = \frac{2\alpha^{\alpha}\beta^{\beta}}{\Gamma(\alpha)\Gamma(\beta)} \frac{1}{I_0} \left(\frac{1}{I_0}\right)^{\alpha-1} \exp(-\beta \frac{1}{I_0}) \quad (1)$$

where I is the optical power received, α and β are shape parameters related to the small- and large-scale turbulence effects, Γ(.) denotes the gamma function and I_0 is a normalization constant related to the average optical power received. Parameters α and β can be determined based on the strength of atmospheric turbulence, characterized by the refractive index structure parameter C_n^2, the propagation distance L and the wavelength λ.

The expressions for the parameters α and β are given by:

$$\alpha = \left(exp\left(\frac{0.49\sigma_R^2}{\left(1+1.11\sigma_R^{12/5}\right)^{7/6}} \right) - 1 \right)^{-1} \quad (2)$$

$$\beta = \left(exp\left(\frac{0.51\sigma_R^2}{\left(1+0.69\sigma_R^{12/5}\right)^{5/6}} \right) - 1 \right)^{-1} \quad (3)$$

The strength of atmospheric turbulence is often quantified by the Rytov variance, denoted by σ_R^2. For a plane wave propagating through the atmosphere, the Rytov variance is given by [53]:

$$\sigma_R^2 = 1.23 C_n^2 k^{7/6} L^{11/6} \quad (4)$$

where C_n^2 is the refractive index structure parameter, indicating the strength of turbulence, $k = \frac{2\pi}{\lambda}$ is the number of optical waves, λ is the wavelength of the optical signal and L is the length of the propagation path.

In vertical FSO communication, the calculation of atmospheric turbulence becomes more complicated due to the varying refractive index with height. The refractive index structure parameter (C_n^2) measures the intensity of refractive-index fluctuations in the atmosphere and varies both spatially and temporally. Higher C_n^2 values indicate more turbulence, leading to increased scintillation and signal loss in optical communication.

Using the Hufnagel-Valley model, the fluctuation of the refractive-index structure parameter $C_n^2(h)$ with altitude h is expressed as ([54]):

$$C_n^2(h) = 0.00594\left(\frac{v_{wind}}{27}\right)^2 (10^{-5}h)\exp\left(-\frac{h}{1000}\right) + 2.7\times10^{-16}\exp\left(-\frac{h}{1500}\right) + C_n^2(0)\exp(-\frac{h}{100}) \quad (5)$$

where, $C_n^2(0)$ is the level of ground turbulence, ranging from 10^{-17} $m^{-2/3}$ (weak turbulence) to 10^{-13} $m^{-2/3}$ (strong turbulence) and v_{wind} (m/s) is the mean squared root wind speed, typically around 21 m/s.

3.2 Cloud Attenuation Analysis

The presence of liquid-water particles in clouds has a significant impact on FSO communication with atmospheric conditions. When laser beams pass through the Earth's atmosphere, these small-scale components cause light waves to scatter in multiple directions, inhibiting coherent transmission. Cloud-induced scattering has a significant impact on visibility, which is a crucial factor in evaluating the effectiveness of optical-communication systems. Visibility, measured in kilometers, is a quantifiable measure of the clarity and transparency of the atmosphere. The loss of signal power in FSO networks caused by cloud scattering's effect on vision indicates that the optical transmission conditions are insufficient. In [35], the authors provided many types of cloud with variable attenuation effects, as depicted in Figure 1. Table 2 compares their impacts on the FSO signal.

- Cirrus, cirrostratus and cirrocumulus are high-altitude clouds. These clouds, which exist at high elevations and low temperatures, help to reduce solar radiation and maintain a delicate balance of thermal exchanges in the Earth's atmosphere.
- Altocumulus and altostratus are mid-level clouds that migrate at high and low altitudes. Their role in controlling solar radiation is crucial, as they have a transitional effect on thermal dynamics that determines surface temperatures and atmospheric conditions.
- Cumulus, stratus and stratocumulus are the most common low-level clouds. These clouds, located closer to the Earth's surface, play a crucial role in temperature regulation and atmospheric stability. Cumulus clouds, with their puffy and distinct appearances, denote fair weather, whereas stratus clouds, with their blanket-like patterns, typically imply cloudy conditions. Stratocumulus clouds have both stratus and cumulus features and act as transitory elements in meteorological processes.
- Raining clouds are multi-layered clouds that appear at all levels of the atmosphere. This classification includes nimbostratus and cumulonimbus clouds. Nimbostratus clouds generate huge, featureless strata linked by persistent precipitation, contributing to the replenishment of the Earth's water resources. Cumulonimbus clouds, popularly known as the "king of clouds," spread across multiple atmospheric strata, encapsulating dynamic convective processes that create severe weather events, such as thunderstorms and heavy rainfall.

Equation (6) shows how to determine visibility based on the concentration of the number of cloud droplets (Nc) and the content of liquid cloud water (CLWC).

$$V = \frac{1.002}{(L\times Nc)^{0.6473}} \quad (6)$$

where L (g/m^3) represents the mean CLWC and Nc (cm^{-3}) denotes the concentration of cloud droplet number [55].

Figure 2 shows the impact of different types of cloud on visibility, including stratus (Nc = 250 cm^{-3}), altostratus (Nc = 400 cm^{-3}) and nimbostratus (Nc = 200 cm^{-3}). Figure 2 also shows a rapid decline in visibility as CLWC increases.

For a mono-dispersed droplet distribution, Equation (7) can be used to calculate the concentration of cloud droplets.

$$Nc = \frac{L}{\frac{4}{3}\Pi r^3\rho\times10^{-6}} \quad (7)$$

where (ρ = 1 g/cm3) signifies the density of liquid water and $r(\mu m)$ represents the average radius of cloud droplets. The value varies with cloud type, such as stratus (r = 3.33μm), nimbostratus (r = 4.7μm) and cumulus (r = 6.0μm) ([57]).

Equation (8) expresses the total cloud attenuation in the cloud layers considered, indicated as A_c (dB),

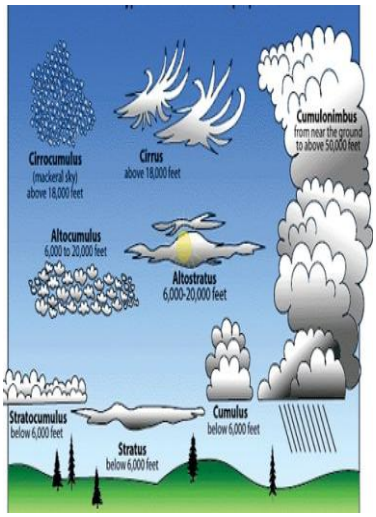

Figure 1. Cloud types.

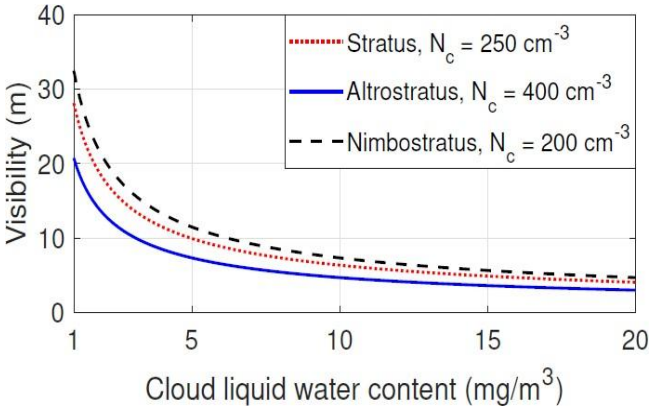

Figure 2. Visibility for several cloud types [56].

using visibility V (km) in Equation (6) and the Kim model [51] to represent the attenuation due to Mie scattering.

$$A_c = \sum_{k=1}^{M} 4.34 \left(\frac{3.91}{V_k}\left(\frac{\lambda}{550}\right)^{-\delta_k}\right) \frac{\Delta h_k}{\sin(\theta)} \tag{8}$$

where λ is the optical wavelength, θ is the elevation angle of the satellite, M is the total layers of the cloud investigated and Δh_k is the vertical extent of the layer of liquid clouds k^{th} ([58]). Furthermore, the coefficient δ, which depends on the size distribution of the scattering particles, is estimated using empirical models [59] and provided by the Kim model as follows.

$$\delta_k = \begin{cases} 1.6 & if\ V > 50km \\ 1.3 & if\ 6km < V < 50km \\ 0.16V + 0.34 & if\ 1km < V < 6km \\ V - 0.5 & if\ 0.5km < V < 1km \\ 0 & if\ V < 0.5km \end{cases} \tag{9}$$

Table 2. Cloud-type comparison.

Cloud Type	Height Range	FSO Attenuation	CLWC (g/m^3)	Optical Thickness
Stratus	Low altitude	Moderate attenuation	0.28 [35]	Moderate to high
Cumulus	Moderate altitude	Low attenuation	0.26 [35]	Low to moderate
Cumulonimbus	Low to high altitude	High attenuation	1 [35]	High
Stratocumulus	Low to middle altitude	Moderate attenuation	0.44 [35]	Moderate
Cirrus	High altitude	Low attenuation	0.03 [35]	Low

3.3 Combining Atmospheric Turbulence and Cloud Attenuation

The performance of Free-Space Optical (FSO) communication systems is significantly influenced by atmospheric turbulence and cloud attenuation, which collectively degrade the quality and reliability of optical links. Understanding the combined effect of these environmental factors is essential for designing robust FSO systems capable of maintaining reliable communication under varying weather conditions.

The combined effect of atmospheric turbulence and cloud attenuation on the FSO channel can be mathematically expressed as follows:

$$P_{\text{received}} = P_{\text{transmitted}} \cdot e^{-\alpha L} \cdot e^{-\beta C_n^2 L^{5/3}} \tag{10}$$

where, P_{received} is the received optical power after propagation through the atmosphere, accounting for both cloud attenuation and atmospheric turbulence, while $P_{\text{transmitted}}$ is the optical power transmitted

from the FSO transmitter. The coefficient α represents the attenuation due to clouds, which is influenced by the optical depth, density and type of the cloud (e.g. cirrus, cumulus) [51]. The term β is the turbulence coefficient that quantifies the effect of atmospheric turbulence on the received signal, C_n^2 being the refractive-index structure parameter [52]. Finally, L denotes the propagation distance through the atmosphere.

In this equation, the term $e^{-\alpha L}$ accounts for the exponential attenuation of the optical signal due to clouds along the propagation path. The coefficient α depends on the optical depth and scattering properties of the clouds, which affect the amount of incident light that reaches the FSO receiver [51].

The term $e^{-\beta C_n^2 L^{5/3}}$ represents the Rytov-based model of turbulence-induced fading in the presence of atmospheric turbulence. The coefficient β characterizes the strength of turbulence, while C_n^2 quantifies the spatial and temporal variations in the refractive index caused by turbulence [52]. The exponent $L^{5/3}$ reflects the scaling of turbulence effects with propagation distance L, highlighting the increasing impact of turbulence on signal degradation over longer distances [51].

Cloud attenuation and air turbulence can have a substantial impact on the reliability and quality of FSO communication systems. Because clouds can significantly reduce signal quality, real-time monitoring and adaptive techniques are critical for increasing the overall system performance. Advanced modulation algorithms, error-correction coding and dynamic link adaptability are crucial to improving the resilience of FSO systems under a variety of weather conditions.

4. GROUND TO SATELLITE FSO SYSTEM

4.1 System Design

In this sub-section, we use Optisystem software to develop a ground-satellite FSO system that operates under turbulence and various cloud circumstances. OptiSystem was selected because of its ability to provide a comprehensive and realistic simulation of free-space optical (FSO) communication systems by incorporating key physical impairments. These include atmospheric turbulence effects, which are modeled using the gamma–gamma turbulence distribution and cloud-induced attenuation, integrated through empirical models based on Mie scattering theory. In addition, the software offers accurate optical component modeling, enabling a precise evaluation of modulation techniques and signal-quality metrics. In our simulation, we investigate various modulation methods for reducing cloud and turbulence impacts in optical ground-to-satellite communication. Table 3 summarizes the simulation parameters and their respective values.

Our simulations target ground-to-satellite links over extreme distances (up to 35,000 km), where loss of free-space path, atmospheric attenuation and turbulence impose severe challenges. We selected a link distance range from 2000 km to 36000 km to focus on the most challenging conditions in long-range FSO communications. Although shorter links (e.g. 500 km) experience significantly lower losses and reduced atmospheric effects, our study targets scenarios where severe free-space path loss, atmospheric attenuation and turbulence dominate. Established literature confirms that performance degradation becomes critical above 2000 km, justifying our focus on this range to ensure that our system design, particularly in terms of transmitter power and receiver aperture, is validated under the most extreme conditions encountered in ground-to-satellite and inter-satellite links. Under such harsh conditions, a higher transmit power is essential to maintain an acceptable signal-to-noise ratio (SNR) and achieve a low bit-error rate (BER). This design choice is supported by established link-budget analyses; for example, [60] demonstrated that long-range FSO links require elevated power levels to overcome significant path losses and [46] provided a detailed analysis that reinforces the need for higher transmission power in ground-to-satellite transmissions. Although lower transmit power might suffice for terrestrial FSO systems, the unique challenges of space-to-ground links justify our approach, ensuring that our simulation accurately reflects the operational demands of these systems.

Figure 3 shows a ground-to-satellite FSO system with an uplink from a ground station to a geostationary satellite. FSO links provide high-speed communication between satellites and ground stations. However, certain meteorological circumstances encountered during uplink transmission, including cloud attenuation and atmospheric turbulence, can have a major impact on the FSO link's performance. Cloud attenuation occurs when clouds absorb, scatter and refract laser beams, causing

signal attenuation. Another key difficulty is atmospheric turbulence, which occurs when air masses move irregularly, creating temperature and pressure variations. These fluctuations cause variations in the refractive index of the atmosphere, resulting in scintillation effects on laser beams. Mitigating the effects of atmospheric turbulence is critical for stabilizing FSO lines and maintaining constant signal quality.

Table 3. Simulation parameters.

Parameters	Value
Pre-amplification gain	30 (dB)
Post-amplification gain	30 (dB)
Noise-figure pre-amplification	5 (dB)
Noise-figure post-amplification	3 (dB)
Transmit power	0-50 (dB)
Transmitter diameter	5 (cm)
Receiver diameter	30 (cm)
Data rate	30 (Gb/s)
Link distance	2000-36000 (km)
Photo-detector responsitivity	1 (A/W)
Laser wavelength	1550 (nm)
Tropopause height	9.4 (km)
Turbulence model	Hafmagel Valley Model
Refractive-index structure	$C_n^2(0)$ Turbulence close to ground (strong turbulence: $C_n^2(0) = 2.10^{-13} m^{-2/3}$)

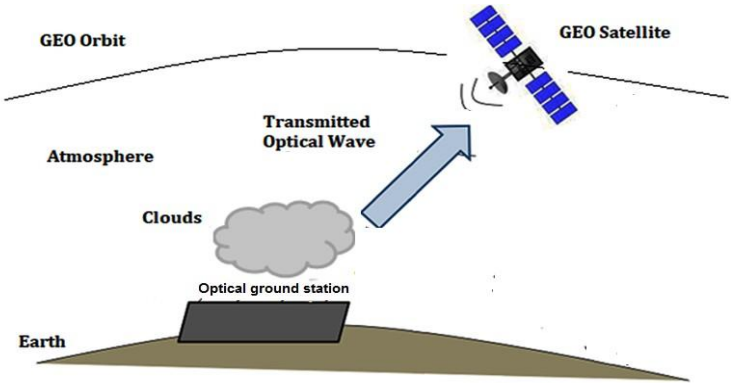

Figure 3. Satellite-to-ground FSO system.

In addition, 30 cm receiver diameter was selected to overcome the substantial free-space loss and atmospheric attenuation inherent in ground-to-satellite FSO links over long distances. Although terrestrial FSO systems commonly operate with receiver diameters in the 5–10 cm range, space-based optical ground stations often employ larger apertures to collect much weaker signals from vast distances. For example, NASA's Lunar Laser Communication Demonstration (LLCD) used a receiver telescope with an aperture of the order of 40 cm to ensure sufficient signal collection from the Moon [61]. Furthermore, detailed link-budget analyzes for free-space optical satellite networks indicate that larger receiver diameters are necessary to achieve the signal-to-noise ratio (SNR) required over such long distances [46]. Therefore, our choice of a 30 cm receiver diameter is both practical and consistent with established approaches in long-range space optical communications.

The ground-to-satellite FSO channel consists of two serially coupled channels. The first FSO channel that simulates the atmosphere is 12 kilometers long. The length of the atmospheric channel is determined by averaging the tropopause elevation, which is 9 km at the pole and 15 km at the equator ([62]). The tropopause marks the boundary between the troposphere and the stratosphere. The troposphere accounts for 75% of the atmosphere's mass and 99% of the total mass of water vapor and aerosols ([62]). This FSO channel represents the atmosphere and simulates the attenuation induced by various types of cloud and atmospheric turbulence. The second FSO channel depicts a space channel

with a length of 35,988 kilometers. Because it depends solely on beam divergence and transmitter-receiver aperture diameter, it is only useful for geometric loss, which has a fixed value.

4.2 Modulation Approaches for the Proposed Ground-Satellite FSO System

The choice of modulation method is crucial to maintaining the reliability and efficiency of data transmission in a high-speed FSO communication system operating at 30 Gbps, especially when dealing with cloud interference. This sub-section presents advanced modulation techniques, such as QPSK, 8-PSK, 16-PSK and 16-QAM. We selected QPSK, 8-PSK, 16-PSK and 16-QAM for the following reasons:

- QPSK (Quadrature Phase Shift Keying): QPSK is widely recognized for its robustness against signal degradation, particularly in high-attenuation environments caused by clouds and atmospheric turbulence. It offers a balance between data rate and resistance to errors, making it optimal for low- to-moderate signal-to-noise ratio conditions. This makes QPSK particularly suitable for satellite communication links, where maintaining low bit error rates (BER) is crucial.
- Higher-order Modulation Schemes (8-PSK, 16-PSK, 16-QAM): These modulation techniques provide higher spectral efficiency than QPSK, allowing for greater data throughput within the same bandwidth. 8-PSK and 16-PSK use phase variations to encode data, while 16-QAM adds both amplitude and phase variations, allowing the encoding of even more information in a given symbol. While these schemes offer higher data rates, they are also more susceptible to noise and signal impairments, especially in turbulent or attenuated atmospheric conditions.

4.2.1 M-PSK Modulation

M-PSK divides the signal's phase into M distinct states, each corresponding to a specific bit combination. Phases are often uniformly distributed throughout the signal constellation, creating a distinct pattern. In binary phase-shift keying (BPSK), there are two phase states at 0 and 180 degrees, while in quadrature phase-shift keying (QPSK), there are four phase states spread at 90-degree intervals. M-ary Phase Shift Keying (M-PSK) modulation is more advanced than binary methods, because it uses higher-order modulation methods, such as 8-PSK and 16-PSK to effectively encode digital data onto a carrier signal. Figure 4 shows the design of the M-PSK system. 8-PSK divides the phase of the carrier signal into eight equidistant states, each representing a distinct three-bit pattern. Phase states are usually 45 degrees apart, enabling the transmission of three bits per symbol. This increase in spectral efficiency is especially beneficial in situations where a greater data rate is necessary. 8-PSK achieves a compromise between enhanced capacity and controllable complexity, making it a pragmatic option in digital communication systems. 16-PSK increases complexity by segmenting the phase of the carrier signal into sixteen states, each separated by 22.5 degrees. Higher data-transmission rates are achieved as a result of being able to convey a distinct four-bit pattern with every phase state.

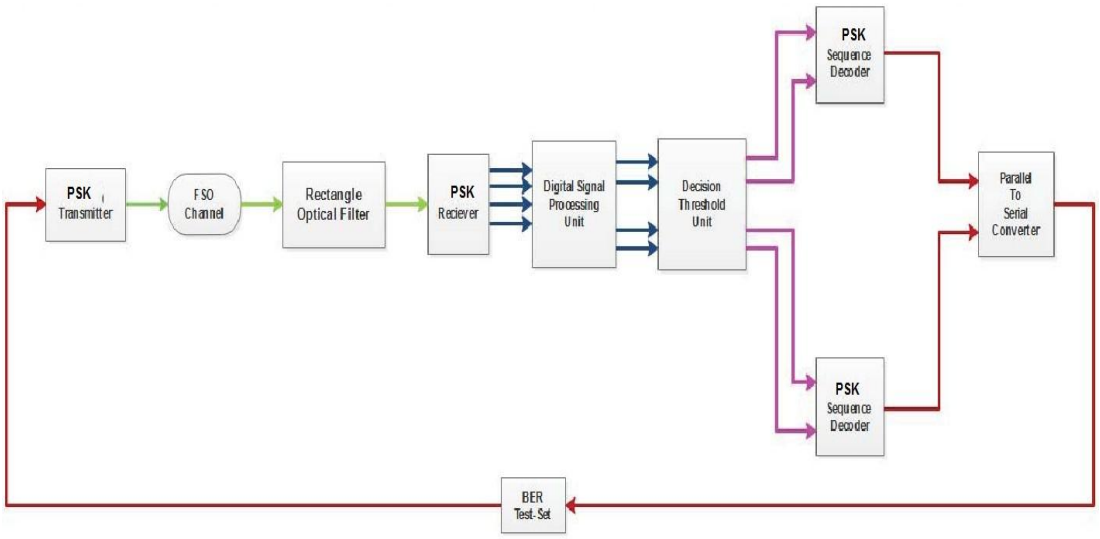

Figure 4. M-PSK system design.

4.2.2 M-QAM Modulation

Optical M-QAM (M-ary Quadrature Amplitude Modulation) is a modulation scheme used in optical-communication systems to encode digital information onto an optical carrier wave. Figure 5 illustrates the design of the M-QAM system. The concept combines both amplitude and phase modulation to achieve higher spectral efficiency. In M-QAM, the amplitude and phase of the optical signal are modulated simultaneously, allowing for the transmission of multiple bits per symbol. The "M" in M-QAM denotes the number of different states in the signal constellation, representing unique combinations of amplitude and phase. For example, in 16-QAM, there are 16 different states, enabling the representation of 4 bits per symbol. The optical signal's amplitude and phase states are typically arranged in a square or rectangular constellation, with the states positioned at specific points in the complex plane.

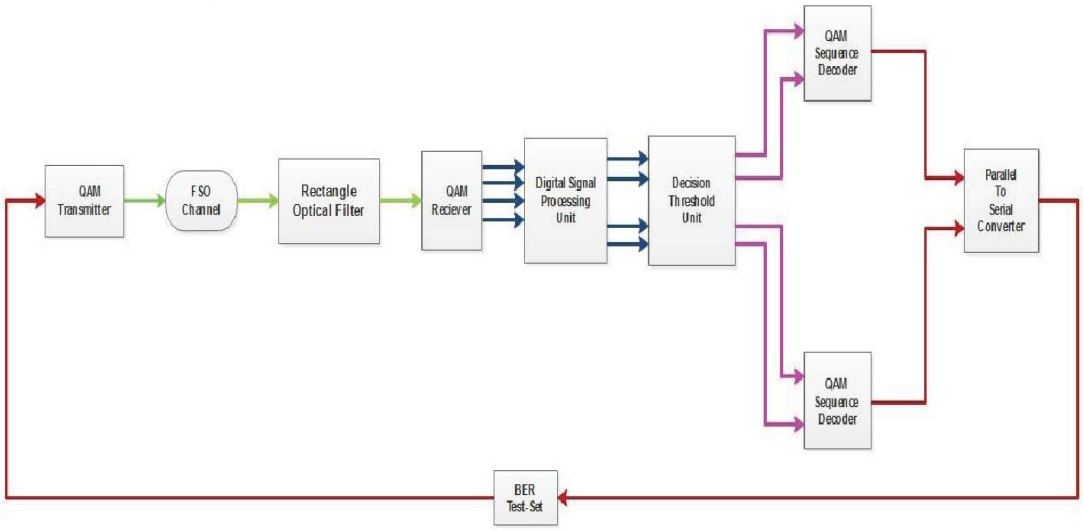

Figure 5. M-QAM system design.

5. SIMULATION RESULTS

In this section, we evaluate the performance of the proposed ground-satellite-ground FSO communication system under different cloud conditions and under strong turbulence.

Figure 6 illustrates the quality factor for different modulation schemes (QPSK, 8-PSK, 16-PSK and 16- QAM) at varying link distances. At a link distance of 2000 km, all modulation schemes exhibit relatively high quality-factor values. In particular, QPSK and 16-PSK demonstrate robust performance, possessing higher quality factors compared to 8-PSK and 16-QAM in this short range.

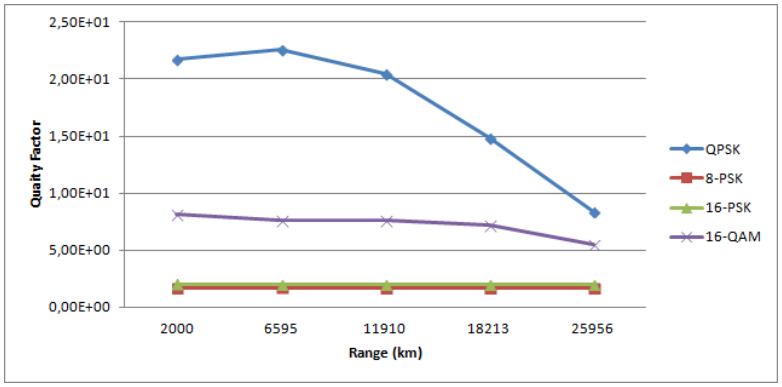

Figure 6. Quality factor *vs*. link distance (km).

The superior performance of QPSK and 16-PSK can be attributed to their enhanced tolerance to noise and channel impairments, resulting from larger symbol separations. This is contrasted with 8-PSK and 16-QAM, the denser constellation arrangements of which lead to higher susceptibility to noise even when SNR is high. These findings underscore the trade-off between spectral efficiency and robustness,

reinforcing our conclusion that QPSK, in particular, is the most robust modulation scheme for ground-to-satellite FSO links under adverse atmospheric conditions. As the link distance increases, a general trend of decreasing quality-factor values emerges across all modulation schemes. The decline in the quality factor indicates the sensitivity to distance-induced signal degradation and the varying rates of decrease among modulation schemes highlight differences in their resilience to longer link distances.

Figure 7 shows the BER obtained for different modulation schemes (QPSK, 8-PSK, 16-PSK and 16-QAM) at different levels of attenuation. Each attenuation value corresponds to a cloud type, as described in Table 4.

Table 4. Attenuation at 1550nm of different types of cloud.

Cloud Type	Attenuation (dB/km)
Stratus	0.035
Cumulus	0.037
Cumulonimbus	0.011
Stratocumulus	0.026
Cirrus	0.134

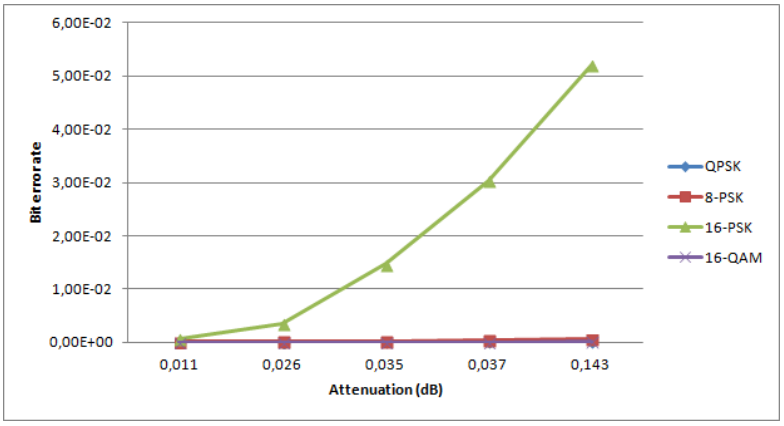

Figure 7. BER *vs*. attenuation (dB).

QPSK consistently exhibits lower BER values, making it more robust and less susceptible to errors induced by signal attenuation. 16-QAM experiences a comparatively higher BER compared to QPSK, 8-PSK and 16-PSK at an attenuation level of 0.143, indicating that it may be more sensitive to higher levels of attenuation, making it less robust under challenging communication conditions. 8-PSK and 16-PSK have moderate sensitivity to attenuation, indicating a trade-off between higher data rates and increased susceptibility to signal degradation.

To statistically characterize the fluctuations induced by turbulence in the intensity received I, we employ the gamma–gamma distribution. Its probability density function is given by:

$$p_I(I) = \frac{2(\alpha\beta)^{\frac{\alpha+\beta}{2}}}{\Gamma(\alpha)\Gamma(\beta)} I^{\frac{\alpha+\beta}{2}} K_{\alpha-\beta}\left(2\sqrt{\alpha\beta\frac{I}{I_0}}\right) \quad (11)$$

where, α and β are parameters related to the small-scale and large-scale turbulence effects, I_0 is the average received power, $\Gamma(\cdot)$ denotes the gamma function and $K_v(\cdot)$ is the modified Bessel function of the second kind.

This model allows us to derive the effective signal-to-noise ratio (SNR), γ_{eff}, which is used to compute the bit-error rate (BER) through the Q function:

$$\text{BER} = Q\left(\sqrt{\gamma_{eff}}\right) \quad (12)$$

Figure 8 illustrates the BER for various modulation schemes, including QPSK, 8-PSK, 16-PSK and 16- QAM, at different communication ranges. We note that at shorter ranges, such as 2000 km and 6595km, both QPSK and 16-QAM exhibit BER of 0, indicating reliable and error-free performance within these distances. On the other hand, 8-PSK and 16-PSK, while maintaining relatively low BER values, show slightly higher error rates compared to QPSK and 16-QAM in these short ranges. The QPSK modulation technique demonstrates robustness throughout the entire range, consistently

delivering lower BER values compared to the other modulation schemes. This underscores the suitability of QPSK for scenarios that require reliable communication over extended distances.

Thus, at shorter distances, such as 2000 km and 6595 km, the free-space path loss and turbulence-induced fading are minimal, resulting in a higher received signal power and a correspondingly high signal-to-noise ratio. Under these favorable conditions, the system operates in an optimal regime, where the channel impairments are negligible. This shows that when the channel is not significantly stressed by attenuation or noise, even more complex modulation schemes can achieve near-perfect decoding.

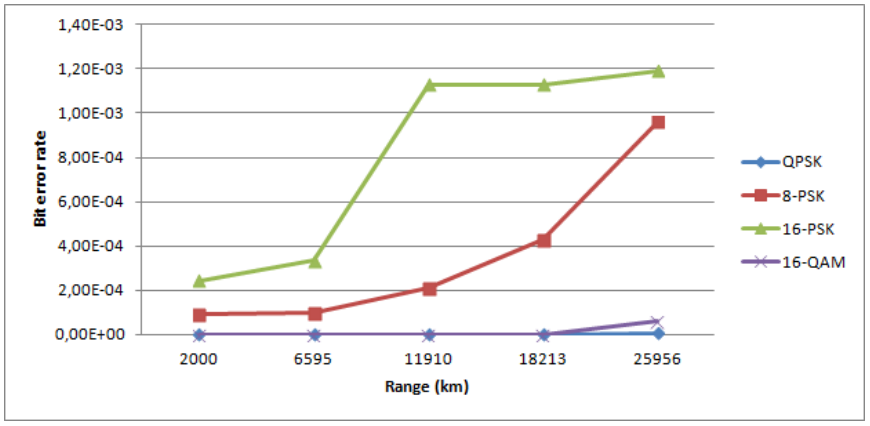

Figure 8. BER *vs*. link distance (km).

In addition to the BER and OSNR, we evaluate the performance of the FSO system using the quality factor Q. The quality factor quantifies the separation between the signal and noise levels and is defined as:

$$Q = \frac{\mu_{\text{signal}} - \mu_{\text{noise}}}{\sigma_{\text{signal}} + \sigma_{\text{noise}}} \tag{13}$$

where μ_{signal} and μ_{noise} denote the mean values of the signal and noise, respectively, and σ_{signal} and σ_{noise} represent their corresponding standard deviations. A higher Q value implies a clearer distinction between the signal and noise, which generally corresponds to a lower bit-error rate (BER).

Figure 9 describes the BER *versus* the transmitted power for various modulation schemes, including QPSK, 8-PSK, 16-PSK and 16-QAM. At a transmitted power of 0, all schemes exhibit BER values around 0.5, except for 16-QAM, which has a slightly higher BER of 0.51. As the transmitted power increases to 10, the BER decreases, with QPSK showing a significant improvement, at a transmitted power of 15, QPSK achieves an exceptionally low BER of 3.00E-05, demonstrating its resilience to errors. At higher transmission-power levels, the BER values consistently approach zero, indicating that higher transmission-power levels contribute to a stronger and more reliable signal, resulting in significantly reduced error rates. QPSK consistently achieves lower BER values across the range of transmitted powers, while 16-QAM appears to be more sensitive to variations in transmitted power, especially at lower levels.

The observed differences in BER performance between modulation schemes can be attributed to the inherent characteristics of their constellation designs and the robustness to noise. QPSK utilizes a four-point constellation with wider Euclidean distances between symbols, making it more resilient to noise and channel impairments. In contrast, 16-QAM compresses 16 symbols into the same signal space, resulting in closer constellation points and increased susceptibility to errors in the presence of noise or power variations. Although higher-order modulation schemes, such as 16-QAM, offer superior spectral efficiency, they suffer from reduced robustness under adverse conditions. This trade-off is evident in our simulations (as seen in Figure 9), where QPSK maintains a lower BER across various transmitted power levels due to its larger decision regions, while 16-QAM exhibits a higher BER in low-power scenarios. These results highlight the fundamental balance between spectral efficiency and signal robustness in FSO-communication systems.

In our model, the received optical power P_{received} is expressed as:

$$P_{\text{received}} = P_{\text{transmitted}} \cdot e^{-\alpha L} \cdot e^{-\beta C_n^2 L^{5/3}} \tag{14}$$

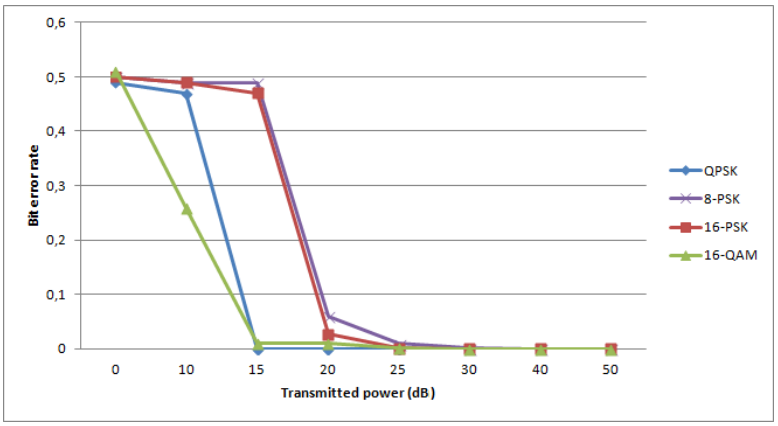

Figure 9. BER *vs*. transmitted power (dB).

where, $P_{\text{transmitted}}$ is the transmitted optical power, L is the link distance, α represents the attenuation coefficient due to clouds (derived from empirical models, such as those based on Mie scattering theory), C_n^2 is the refractive-index structure parameter, characterizing the strength of atmospheric turbulence and β is a scaling constant that captures turbulence-induced fading.

The degradation in received power due to atmospheric turbulence is further characterized by the Rytov variance:

$$\sigma_R^2 = 1.23 C_n^2 k^{7/6} L^{11/6} \tag{15}$$

with $k = \frac{2\pi}{\lambda}$ being the optical wave number and λ the operating wavelength. Under strong turbulence, the factor $e^{-\beta C_n^2 L^{5/3}}$ effectively models the fading effect that affects the received signal.

Figure 10 illustrates the BER in different modulation schemes, including QPSK, 8-PSK, 16-PSK and 16-QAM, at different levels of the OSNR. The OSNR is defined as the ratio of the received optical signal power to the noise power spectral density:

$$\text{OSNR} = \frac{P_{\text{signal}}}{N_0.B} \tag{16}$$

where P_{signal} represents only the power of the transmitted signal (without the noise contribution) contrary to P_{received} which is the optical power detected in the receiver after accounting for losses due to atmospheric and cloud attenuation. N_0 represents the spectral density of the noise power. B is the bandwidth of the channel over which the optical signal and noise are measured. The data shows that at an OSNR of 0, higher BER values are observed, with QPSK demonstrating a lower BER, indicating its robustness in maintaining signal quality. Higher-order modulation schemes, like 16-PSK and 16-QAM, exhibit higher BERs, indicating increased sensitivity to noise. As OSNR increases to 5, 10 and 15, the BER decreases consistently, with QPSK demonstrating superior performance with extremely low BER values. At higher OSNR levels (20 and 25), the BER values approach zero, indicating a substantial reduction in errors. QPSK maintains its advantage with consistently low BER, but even higher-order modulation schemes achieve highly reliable communication under these favorable conditions.

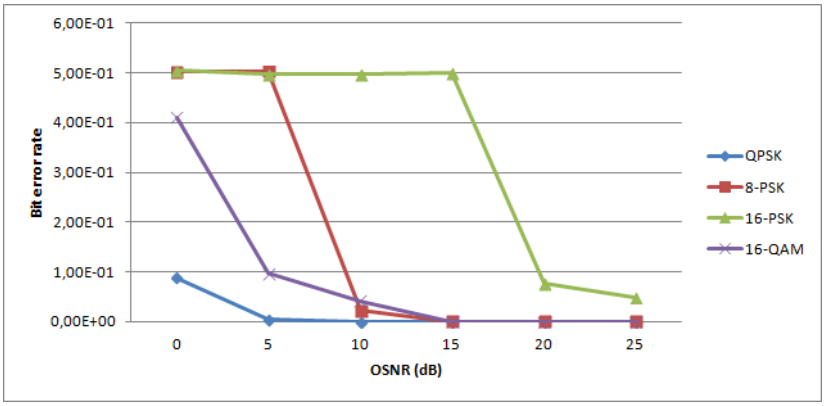

Figure 10. BER *vs*. OSNR (dB).

The trade-off between spectral efficiency and noise robustness plays a critical role in the performance of different modulation schemes in FSO communication. QPSK, with its four-symbol constellation, benefits from larger Euclidean distances between symbols, making it inherently resilient to noise and channel impairments. This ensures a consistently low BER even in challenging conditions. However, higher-order modulation schemes, such as 16-QAM, achieve greater spectral efficiency by packing more symbols into the same signal space. Although this increases data throughput, it also reduces the separation between constellation points, making the modulation more sensitive to noise and signal distortions. However, under optimal conditions, such as high optical signal-to-noise ratio, minimal attenuation and low turbulence, 16-QAM and other higher-order schemes can maintain low BER values due to the reduced impact of noise. This highlights the fundamental trade-off: QPSK remains a robust choice across a wide range of conditions, whereas higher-order modulations can achieve similar performance when the channel provides a high- quality, low-noise environment.

Figure 11 shows the values of the quality factor for different modulation schemes, QPSK, 8-PSK, 16-PSK and 16-QAM, at varying levels of OSNR. At an OSNR of 0, the quality-factor values are relatively high, indicating decent signal quality. However, 16-QAM has the lowest quality factor at this level, suggesting that it is more susceptible to noise. As OSNR increases to 5 and 10, the quality factor improves consistently, with QPSK and 8-PSK exhibiting higher quality factors, while 16-QAM shows a significant improvement, highlighting its ability to benefit from increased OSNR for enhanced signal quality. At OSNRs of 15 and 20, the quality factor continues to increase, with QPSK and 8-PSK maintaining strong performances, while 16-QAM shows a substantial improvement, indicating its ability to achieve higher signal quality at elevated OSNR levels. At the highest OSNR level of 25, QPSK and 8-PSK maintain high quality factors, while 16-QAM achieves a notable improvement.

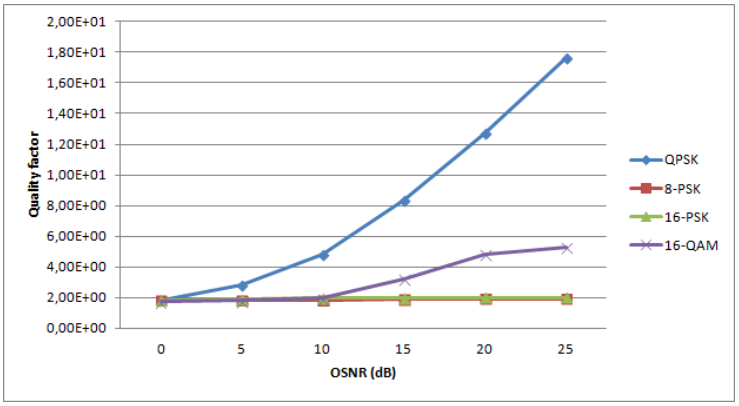

Figure 11. Quality factor vs OSNR (dB).

Figure 12 illustrates the EVM values obtained for different modulation schemes, QPSK, 8-PSK, 16-PSK and 16-QAM, at different levels of OSNR. EVM is calculated by comparing the received optical signal's constellation points to the expected or ideal points based on the modulation scheme used. Lower percentages of EVM indicate a higher fidelity of the received signal to the ideal signal. The relationship between EVM and OSNR provides insight into how signal distortion varies with changes in signal quality for each modulation scheme. At an OSNR of 0, all modulation schemes exhibit relatively high EVM values, indicating significant signal distortion due to low signal-to-noise ratios. Our simulation results indicate that, under optimal atmospheric conditions, 16-QAM can achieve lower EVM values. This suggests that, with effective receiver processing and in low-noise environments, higher-order modulation schemes can also deliver high signal fidelity. As OSNR increases to 5, 10 and 15, the EVM values decrease for all modulation schemes, contributing to improved signal quality and reduced distortion. QPSK and 8-PSK consistently exhibit lower EVM values, demonstrating their resilience even under optimal conditions. Higher-order modulation schemes, such as 16-PSK and 16-QAM, still exhibit higher distortion compared to simpler modulation schemes. Although QPSK typically benefits from a larger decision region, our simulation results indicate that under favorable OSNR conditions, 16-QAM can achieve lower EVM values. This suggests that, with effective receiver processing and in low-noise environments, higher-order modulation schemes can also deliver high signal fidelity.

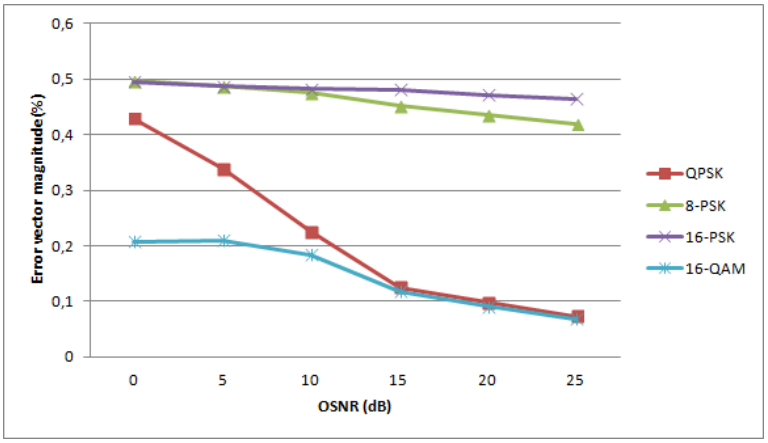

Figure 12. EVM (%) *vs* OSNR (dB).

In conclusion, our study provides a comprehensive evaluation of ground-to-satellite FSO communication systems under realistic atmospheric conditions. The simulation results demonstrate that as the link length increases, the adverse effects of atmospheric turbulence and cloud attenuation become more pronounced, leading to deteriorated performance metrics. Among the modulation schemes analyzed, QPSK emerges as the most robust option, consistently providing lower BER and higher quality factors in high-attenuation scenarios. These insights are critical for designing resilient FSO systems, particularly for satellite-communication applications where maintaining link reliability under extreme conditions is paramount. Future work will explore adaptive modulation strategies and real-world experimental validation to further optimize system performance.

6. List of Abbreviations

Table 5. List of abbreviations.

Abbreviation	Full Form	Abbreviation	Full Form
FSO	Free Space Optical	DWT	Discrete Wavelet Transform
BER	Bit Error Rate	MIMO	Multiple-Input Multiple-Output
OSNR	Optical Signal-to-Noise Ratio	ADC	Analog-to-Digital Converter
SNR	Signal-to-Noise Ratio	DSP	Digital Signal Processing
QPSK	Quadrature Phase Shift Keying	LEO	Low Earth Orbit
8-PSK	8-Phase Shift Keying	GEO	Geostationary Orbit
16-PSK	16-Phase Shift Keying	WDM	Wavelength Division Multiplexing
16-QAM	16-Quadrature Amplitude Modulation OOK On-Off Keying	RF	Radio Frequency
DPSK	Differential Phase Shift Keying	HT	Hilbert Transform
M-PSK	M-ary Phase Shift Keying	C_n^2	Refractive Index Structure Parameter
M-QAM	M-ary Quadrature Amplitude Modulation	MZM	Mach–Zehnder Modulator
LOS	Line of Sight	AWGN	Additive White Gaussian Noise
CWT	Continuous Wavelet Transform	Q	Quality Factor

7. Conclusion

FSO communication is crucial to improve resilience and adaptive capacity to climate-related hazards and natural disasters, with high data rates and low latency. Its applications include telecommunications, disaster response, military communications, scientific research and aerospace. FSO's rapid deployment capabilities and versatility in addressing diverse communication challenges make it essential in regions where traditional infrastructure is impractical or disrupted.

The study examines the challenges faced by FSO technology, particularly in satellite-to-ground communications amid atmospheric obstructions, such as clouds and turbulence. It reveals that QPSK modulation is the optimal choice for FSO communication in satellite networks facing cloud-induced

attenuation. QPSK consistently maintains the lowest BER even in adverse conditions and exhibits exceptional resilience in the face of varying transmitted power and noise levels.

Future research will focus on refining mitigation strategies for cloud effects on FSO system performance, exploring innovative modulation techniques and developing advanced models to quantify atmospheric impacts more accurately. Practical implementation and field testing of the proposed FSO system under real-world conditions would provide valuable insights into its performance and robustness.

REFERENCES

[1] A. U. Chaudhry and H. Yanikomeroglu, "Free Space Optics for Next-Generation Satellite Networks," IEEE Consumer Electronics Magazine, vol. 10, pp. 21-31, 2020.

[2] A. U. Chaudhry and H. Yanikomeroglu, "When to Crossover from Earth to Space for Lower Latency Data Communications?" IEEE Trans. on Aerospace and Electronic Syst., vol. 58, pp. 3962-3978, 2022.

[3] A. U. Chaudhry et al., "Laser Intersatellite Link Range in Free-space Optical Satellite Networks: Impact on Latency," IEEE Aerospace and Electronic Systems Magazine, vol. 38, pp. 4-13, 2023.

[4] S. Magidi and A. Jabeena, "Free Space Optics, Channel Models and Hybrid Modulation Schemes: A Review," Wireless Personal Communications, vol. 119, pp. 2951 – 2974, 2021.

[5] T. Ahmmed et al., "The Digital Divide in Canada and the Role of LEO Satellites in Bridging the Gap," IEEE Communications Magazine, vol. 60, pp. 24-30, 2022.

[6] Z. Ali et al., "Enhanced Learning-based Hybrid Optimization Framework for RSMA-aided Underlay LEO Communication with Non-collaborative Terrestrial Primary Network," IEEE Transactions on Communications, DOI: 10.1109/TCOMM.2024.3465375, 2024.

[7] M. Mrabet and M. Sliti, "Performance Analysis of FSO Communications in Desert Environments," Optical and Quantum Electronics, vol. 56, no. 4, DOI: 10.1007/s11082-024-06315-9, 2024.

[8] M. Sliti and M. Garai, "Performance Analysis of FSO Communication Systems under Different Atmospheric Conditions," Proc. of the 2022 27th Asia Pacific Conf. on Communications (APCC), DOI: 10.1109/apcc60132.2023.10460727, 2023.

[9] S. Magidi and A. Jabeena, "Analysis of Multi-pulse Position Modulation Free Space Optical Communication System Employing Wavelength and Time Diversity over Malaga Turbulence Channel," Scientific African, vol. 12, p. e00777, DOI: 10.1016/j.sciaf.2021.e00777, 2021.

[10] C. a. B. Dath and N. a. B. Faye, "Resilience of Long Range Free Space Optical Link under a Tropical Weather Effects," Scientific African, vol. 7, p. e00243, DOI: 10.1016/j.sciaf.2019.e00243, 2019.

[11] S. Magidi and A. Jabeena, "Parallel Relay-assisted Free-space Optical Communication Using Multi-pulse Position Modulation over the Generalized Turbulence Channel Model," Journal of Optics, vol. 51, no. 1, pp. 133–141, 2021.

[12] J. O. Bandele et al., "Multiple Transmitters for Gain Saturated Pre-amplified FSO Communication Systems Limited by Strong Atmospheric Turbulence and Pointing Error," IEEE Access, vol. 11, pp. 110985-110994, 2023.

[13] M. T. Mbezi et al., "Temperature and Wind Velocity Effects on Bit Error Rate during Free Space Optical Link under Matrix Málaga Turbulence Channel," Sādhanā, vol. 48, pp. 1-6, 2023.

[14] M. T. Mbezi et al., "Variable Antennas Positions Solution to Reduce Pointing Errors Due to Wind Speed and Temperature Coupled Effects During Free Space Optical Link Using Matrix Rician Pointing Error Model," Optica Applicata, vol. 3, pp. 393-406, DOI:10.37190/oa230305, 2023.

[15] E. E. Elsayed, "Performance Analysis and Modeling: Atmospheric Turbulence and Crosstalk of WDM-FSO Network," Journal of Optics, DOI: 10.1007/s12596-024-02434-4, 2021.

[16] E. E. Elsayed, "Performance Enhancement of Atmospheric Turbulence Channels in DWDM-FSO PON Communication Systems Using M-ary Hybrid DPPM-M-PAPM Modulation Schemes under Pointing Errors, ASE Noise and Interchannel Crosstalk," J. Optics, DOI: 10.1007/s12596-024- 01908-9, 2024.

[17] A. Elfikky, M. Soltani and Z. Rezki, "End-to-End Learning Framework for Space Optical Communications in Non-differentiable Poisson Channel," IEEE Wireless Communications Letters, vol. 13, no. 8, pp. 2090-2094, DOI: 10.1109/LWC.2024.3401692, Aug. 2024.

[18] A. Elfikky et al., "Spatial Diversity-based FSO Links under Adverse Weather Conditions: Performance Analysis," Optical and Quantum Electronics, vol. 56, p. 826, DOI: 10.1007/s11082-024-06625-y, 2024.

[19] E. E. Elsayed et al., "Coding Techniques for Diversity Enhancement of Dense Wavelength Division Multiplexing MIMO-FSO Fault Protection Protocols Systems over Atmospheric Turbulence Channels," IET Optoelectronics, DOI: 10.1049/ote2.12111, 2024.

[20] J. O. Bandele, "Performance of Cascaded Gain Saturated and Fixed Gain Optical Amplifier FSO Communication Systems Limited by Scintillation and Pointing Error," Scientific African, vol. 20, p. e01687, DOI: 10.1016/j.sciaf.2023.e01687, 2023.

[21] M. T. Mbezi et al., "Designing of a Quantum TIA to Improve FSO Signal Reception," Scientific

African, vol. 19, p. e01539, DOI: 10.1016/j.sciaf.2022.e01539, 2022.

[22] E. E. Elsayed and B. B. Yousif, "Performance Enhancement of M-ary Pulse-position Modulation for a Wavelength Division Multiplexing Free-space Optical Systems Impaired by Inter-channel Crosstalk, Pointing Error and ASE Noise," Optics Communications, vol. 475, p. 126219, 2020.

[23] H. Kaushal and G. Kaddoum, "Optical Communication in Space: Challenges and Mitigation Techniques," IEEE Communications Surveys and Tutorials, vol. 19, no. 1, pp. 57–96, 2017.

[24] D. Giggenbach and F. Moll, "Scintillation Loss in Optical Low Earth Orbit Data Downlinks with Avalanche Photodiode Receivers," Proc. of the 2017 IEEE Int. Conf. on Space Optical Systems and Applications (ICSOS), pp. 115-122, Naha, Japan, 2017.

[25] L. Luini et al., "Investigation and Modeling of Ice Clouds Affecting Earth-Space Communication Systems," IEEE Trans. on Antennas and Propagation, vol. 66, no. 1, pp. 360–367, 2018.

[26] N. K. Lyras et al., "Cloud Free Line of Sight Prediction Modeling for Optical Satellite Communication Networks," IEEE Communications Letters, vol. 21, no. 7, pp. 1537–1540, 2017.

[27] N. K. Lyras et al., "Cloud Attenuation Statistics Prediction from Ka-band to Optical Frequencies: Integrated Liquid Water Content Field Synthesizer," IEEE Transactions on Antennas and Propagation, vol. 65, no. 1, pp. 319–328, 2017.

[28] T. Nguyen et al., "TCP over Hybrid FSO/RF-based Satellite Networks in the Presence of Cloud Coverage," IEICE Communications Express, vol. 11, no. 10, pp. 649-654, 2022.

[29] P. B. Bhatt et al., "Designing and Simulation of 30Gbps FSO Communication Link under Different Atmospheric and Cloud Conditions," Int. J. of Eng. Trends and Technology, vol. 69, pp. 228-234, 2021.

[30] D. Ko et al., "Cloud Shape and Attenuation Based UAV Trajectory Optimization for FSO Communication," IEEE Transactions on Vehicular Technology, vol. 73, pp. 9911-9926, 2024.

[31] T. V. Nguyen et al., "On the Design of RIS–UAV Relay-assisted Hybrid FSO/RF Satellite–Aerial–Ground Integrated Network," IEEE Trans. on Aerospace and Elect. Syst., vol. 59, pp. 757-771, 2023.

[32] T. V. Nguyen et al., "Link Availability of Satellite-based FSO Communications in the Presence of Clouds and Turbulence," IEICE Communications Express, vol. 10, no. 5, pp. 206–211, 2021.

[33] H. D. Le, T. V. Nguyen and A. T. Pham, "Cloud Attenuation Statistical Model for Satellite-based FSO Communications," IEEE Antennas and Wireless Propagation Letters, vol. 20, no. 5, pp. 643–647, 2021.

[34] P. Bhatt et al., "Designing and Simulation of 30Gbps FSO Communication Link under Different Atmospheric and Cloud Conditions," Int. J. of Eng. Trends and Tech., vol. 69, no.5, pp. 228–234, 2021.

[35] N. Tabassum et al., "Performance Analysis of Free Space Optics Link for Different Cloud Conditions," Proc. of the 2018 4th Int. Conf. on Computing Communication and Automation (ICCCA), DOI: 10.1109/ccaa.2018.8777546, Greater Noida, India, 2018.

[36] N. K. Lyras et al., "Cloud Free Line of Sight Prediction Modeling for Optical Satellite Communication Networks," IEEE Communications Letters, vol. 21, no. 7, pp. 1537–1540, 2017.

[37] M. M. Haque, A. Jahid, M. M. Hasan and P. Das, "Performance of a FSO Link in Presence of Cloud," ULAB Journal of Science and Engineering, vol. 6, no. 1, 2015.

[38] K. Rammprasath and S. Prince, "Analyzing the Cloud Attenuation on the Performance of Free Space Optical Communication," Proc. of the 2013 Int. Conf. on Communication and Signal Processing, DOI: 10.1109/iccsp.2013.6577165, Melmaruvathur, India, 2013.

[39] T. V. Pham et al., "A Placement Method of Ground Stations for Optical Satellite Communications Considering Cloud Attenuation," IEICE Communications Express, vol. 12, no. 10, pp. 568–571, 2023.

[40] J. G. JOlmedo et al., "Visibility Framework and Performance Analysis for Free Space Optical Communications in Satellite Links," IEEE Access, vol. 11, pp. 68897–68911, 2023.

[41] Y. Ata and M. S. Alouini, "Performance of Integrated Ground-Air-Space FSO Links over Various Turbulent Environments," IEEE Photonics Journal, vol. 14, no. 6, pp. 1–16, 2022.

[42] H. Ivanov et al., "Estimation of Cloud-induced Optical Attenuation over Near-Earth and Deep-space FSO Communication Systems," Proc. of the 2021 Int. Conf. on Software, Telecomm. and Computer Networks (SoftCOM), DOI: 10.23919/softcom52868.2021.9559077, Split, Croatia, 2021.

[43] A. K. Sharoar Jahan Choyon and R. Chowdhury, "Performance Comparison of Free-space Optical (FSO) Communication Link under OOK, BPSK, DPSK, QPSK and 8-PSK Modulation Formats in the Presence of Strong Atmospheric Turbulence," J. of Optical Comm., vol. 44, pp. s763 - s769, 2020.

[44] K. Prabu, D. S. Kumar and T. Srinivas, "Performance Analysis of FSO Links under Strong Atmospheric Turbulence Conditions Using Various Modulation Schemes," Optik, vol. 125, pp. 5573-5581, 2014.

[45] M. H. Ibrahim et al., "Effect of Different Weather Conditions on BER Performance of Single-channel Free Space Optical Links," Optik, vol. 137, pp. 291-297, 2017.

[46] J. Liang et al., "Link Budget Analysis for Free-space Optical Satellite Networks," Proc. of the 2022 IEEE 23rd Int. Symposium on a World of Wireless, Mobile and Multimedia Networks (WoWMoM), pp. 471-476, Belfast, UK, 2022.

[47] J. Liang et al., "Free-space Optical (FSO) Satellite Networks Performance Analysis: Transmission Power, Latency and Outage Probability," IEEE Open J. of Vehicular Techn., vol. 5, pp. 244-261, 2021.

[48] J. Liang et al., "Latency *versus* Transmission Power Trade-off in Free-space Optical (FSO) Satellite

Networks with Multiple Inter-continental Connections," IEEE Open Journal of the Communications Society, vol. 4, pp. 3014-3029, 2023.
[49] ECMWF, "ERA-interim Database," Available: https://apps.ecmwf.int/datasets/data/interimfull-daily.
[50] M. Polnik et al., "Scheduling Space-to-Ground Optical Communication under Cloud Cover Uncertainty," IEEE Trans. on Aerospace and Electronic Systems, vol. 57, no. 5, pp. 2838–2849, 2021.
[51] L. C.Andrews and R. L. Phillips, Laser Beam Propagation through Random Media, ISBN: 9780819478320, DOI: 10.1117/3.626196, 2005.
[52] M. A. Al-Habash, "Mathematical Model for the Irradiance Probability Density Function of a Laser Beam Propagating through Turbulent Media," Optical Engineering, vol. 40, no. 8, p. 1554, 2001.
[53] L. C. Andrews, R. L. Phillips and C. Y. Young, "Laser Beam Scintillation with Applications," SPIE eBooks, DOI: 10.1117/3.412858, 2001.
[54] H. Kaushal and G. Kaddoum, "Optical Communication in Space: Challenges and Mitigation Techniques," IEEE Communications Surveys and Tutorials, vol. 19, no. 1, pp. 57–96, 2017.
[55] I. Gultepe, "Fog and Boundary Layer Clouds: Fog Visibility and Forecasting," Birkhäuser Basel eBooks, DOI: 10.1007/978-3-7643-8419-7, 2007.
[56] T. V. Nguyen et al., "On the Design of Rate Adaptation for Relay-Assisted Satellite Hybrid FSO/RF Systems," IEEE Photonics Journal, vol. 14, no. 1, pp. 1–11, 2022.
[57] J. F. Yin et al., "An Investigation into the Relationship between Liquid Water Content and Cloud Number Concentration in the Stratiform Clouds over North China," Atmospheric Research, vol. 139, pp. 137–143, DOI: 10.1016/j.atmosres.2013.12.004, 2014.
[58] M. Alzenad et al., "FSO-based Vertical Backhaul/Fronthaul Framework for 5G+ Wireless Networks," IEEE Comm. Magazine, vol. 56, no. 1, pp. 218–224, DOI: 10.1109/mcom.2017.1600735, 2018.
[59] I. I. Kim et al., "Comparison of Laser Beam Propagation at 785 nm and 1550 nm in Fog and Haze for Optical Wireless Communications," Proc. of SPIE, the Int. Society for Optical Engineering, DOI: 10.1117/12.417512, 2001.
[60] M. A. Khalighi and M. Uysal, "Survey on Free Space Optical Communication: A Communication Theory Perspective," IEEE Communications Surveys & Tutorials, vol. 16, pp. 2231-2258, 2014.
[61] B. S. Robinson et al., "The Lunar Laser Communications Demonstration," Proc. of the 2011 Int. Conf. on Space Optical Systems and Applications (ICSOS), DOI:10.1109/icsos.2011.5783709, 2011.
[62] D. F. Rex, "Climate of the Free Atmosphere," Elsevier eBooks, vol. 4, [Online], Available: http://ci.nii.ac.jp/ncid/BA0097239X, 1969.

ملخص البحث:

يُعدّ الاتّصال الضّوئي في الفضاء الحرّ حلاً لتلبية الطّلب المتزايد على الاتّصالات من القمر الصّناعي؛ فهو يحقّق فوائد منها معدّلات بيانات أعلى وأمان أفضل. لكنّ أداء الاتّصال الضّوئي في الفضاء الحرّ يتأثر بالظّروف المناخية، مثل تشكُّل الغيوم، والاضطراب الجوّي، والتي تتسبّب في إضعاف الإشارة وتشتُّتها إضافةً الى تشوّهات الطّور. ومن الأمور الأساسية أنّ الفهم الأفضل لتأثيرات الظّروف الجوّية على أداء أنظمة الاتّصال الضّوئي في الفضاء الحرّ إلى جانب تبنّي استراتيجيات ناجعة للحدّ من هذه التّأثيرات تعدّ جوهرية وحاسمة لضمان أداءٍ آمنٍ وفعّال لتلك الأنظمة.

في هذه الدّراسة، قمنا بتقييم أداء أنظمة الاتّصال الضّوئي في الفضاء الحرّ تحت ظروف جوّية مختلفة من حيث الاضطراب الجوّي وتشكُّل الغيوم وأنواعها، مع التّركيز على أنظمة الاتّصال من الأرض إلى القمر الصّناعي. وقد عملنا على تحليل العديد من تقنيات التّعديل والمقارنة بينها لمعرفة التّطبيقات التي تلائمها كل تقنية من تقنيات التّعديل. وتسهم النّتائج الّتي تمّ الحصول عليها في توفير رؤىً حاسمة من أجل تحسين استراتيجيات التعديل؛ من أجل الحصول على روابط ضوئية تتّسم بالمتانة والموثوقية بين الأرض والأقمار الصّناعية.